UDK 669.715:539.378.2:52-335.5
Original scientific article/Izvirni znanstveni članek

ISSN 1580-2949
MTAEC9, 57(5)519(2023)

EFFECT OF DIFFERENT APPLICATION PRESSURES ON ROTARY-FRICTION-WELDED AA2024-T6 JOINTS

VPLIV UPORABE RAZLIČNIH TLAKOV NA ZVARE AA2024-T6, IZDELANE S POSTOPKOM VRTILNO-TRENJSKEGA VARJENA

Serkan Apay[1], Fatih Özen[2*], Volkan Onar[3]

[1]Faculty of Engineering, Department of Mechanical Engineering, Düzce University, 81620 Düzce, Turkey
[2]Beşiri Organized Industrial Zone Vocational College, Batman University, 72000 Batman, Turkey
[3]Faculty of Technology, Pamukkale University, Department of Mechanical and Manufacturing Engineering, 20260 Denizli, Turkey

Prejem rokopisa – received: 2023-03-23; sprejem za objavo – accepted for publication: 2023-06-29

doi:10.17222/mit.2023.834

An AA2024-T6 aluminium alloy was welded with a rotary-friction-welding technique using different forging pressures under constant friction pressure. It was found out that the increasing forging pressure has an adverse effect on the tensile strength of the welded joint. The maximum tensile strength was 366.22 MPa for a forging pressure of 80 MPa. However, the failure energies and elongations were decreased as the forging pressure increased. The minimum elongation was 15.45 %, while the minimum failure energy was 4.35 J with a forging pressure of 120 MPa. This situation is attributed to the loss of ductility up to a degree in high forging pressures and temperatures induced in the HAZ. In microstructural examinations the existence of the S phase has dominant role in determining the local hardness. The S phase is affected by the welding heat in the heat-affected zone, the thermomechanically affected zone and the dynamically recrystallized zone. The hardness is increased up to the middle of the TMAZ. In this zone the heat input caused an aging effect and increased the dispersed S phase in the intergranular zones. The aging mainly governed by the heat input increased the hardness up to beginning of the recrystallization zone.

Keywords: AA2024, rotary friction welding, forging pressure

Avtorji v članku opisujejo medsebojno rotacijsko-trenjsko varjenje palic premera 12 mm iz Al zlitine AA2024-T6 s pomočjo tehnike različnih kovaških tlakov in konstantnega tlaka trenja. Avtorji so ugotovili, da naraščajoči kovaški tlak škodljivo vpliva na natezno trdnost zvarnih spojev. Maksimalno natezno trdnost zvara so dosegli pri kovaškem tlaku 80 MPa in sicer 366,22 MPa. Vendar pa se energija porušitve in rastezek zmanjšujeta z naraščanjem kovaškega tlaka. Najmanši vrednosti raztezka15,45-% in najmanjša energija porušitve 4,35 J sta bili doseženi pri tlaku 120MPa. Te razmere avtorji pripisujejo zmanjšanju duktilnosti pri visokem kovaškem tlaku in induciranim temperaturam v toplotno vplivani coni (HAZ; angl.: heat affected zone). Mikrostrukturne preiskave so pokazale, da ima prevladujočo vlogo na lokalno trdoto prisotnost sulfidne faze. Nanjo vpliva toplota, nastala med trenjskim varjenjem v toplotno vplivani coni, termodinamsko vplivani coni (TMAZ) in coni dinamične rekristalizacije. Trdota narašča do sredine TMAZ. V tej coni vnos toplote povzroča učinek staranja in povečano porazdelitev sulfidne faze na meje kristalnih zrn. Staranje je v glavnem kontrolirano z vnosom toplote in trdota v zvaru narašča do začetka rekristalizacijske cone.

Ključne besede: Al zlitinaAA2024, rotacijsko-trenjsko varjenje, kovaški tlak

1 INTRODUCTION

The aluminium alloy AA2024 is a member of the heat-treatable aluminium series.[1] Al-Cu precipitation is the main strengthening mechanism in the Aluminium 2xxx series. AA2024 has good fracture toughness, high corrosion resistance and specific strength.[2] This alloy is generally employed in lightweight applications to save weight such as in airplanes, spacecraft, and high-speed trains.[3,4]

Since the 2xxx series has a high thermal conductivity, a high thermal expansion coefficient and a low melting point, they are hard to weld with traditional welding methods.[5] Therefore, solid-state welding techniques to weld aluminium alloys is of high importance.[6] Among the solid-state welding techniques, rotation friction welding (RFC) is a promising method, especially for the parts with cylindrical cross-section Department of Machinery and Metal Technologies, s.[7–9] In RFC, two cylindrical cross-section materials are forced to rotate to generate heat with the pressure applied by axial forces.[10–13] This technique can be regarded as a relatively quick technique that generally lasts for tens of seconds.[14,15]

Since the principles of friction welding are the same, there are some variants of this welding method such as friction stir welding (FSW), linear friction welding (LFW), and rotary friction welding (RFW). There are also various studies regarding friction welding in the literature.[17–19] Prashanth and others studied RFW of Al–12Si parts manufactured with the selective laser melting method.[16] The shape and size of the Si phase increased in the weld zone. This variation has resulted in significant changes to the mechanical properties of the weld joint. Rafi and others investigated the mechanical and microstructural properties of RFW applied to a AA7075-T6 joint.[17] They found that the spindle speed, friction pressure, and burn-off length affect the joint strength with 89% joint efficiency. Mogami and others

*Corresponding author's e-mail:
fatih.ozen@batman.edu.tr (Fatih Özen)

investigated high-frequency LFW of 5052 and 6063 aluminium alloys.[18] Material flow during welding was affected by the thermal conductivity at elevated temperatures. They also noted that the grains are refined and the hardness was increased at the interface of the Al 6063 alloy. The joints with low heat inputs yielded higher joint strengths.

In this work AA2024-T6 aluminium rod materials were welded with a rotary-friction-welding technique. The effect of forging pressure under constant parameters were investigated. Tensile tests were applied to rotary-friction-welded specimens. Failure energies, elongations and tensile results were evaluated in terms of different forging pressures. The microstructure was characterized by optical microscope, SEM, SEM/EDS devices. Phase formations was evaluated and supported by the literature.

2 MATERIALS AND METHOD

In this study, AA2024-T6 with an 18-mm diameter was employed. The specimens were machined to 12-mm. The tensile tests were performed on a SHIMADZU AGS-50kN Universal testing device according to the ATSM E8 standard. The crosshead speed was adjusted to 5 mm·min^{-1}. The tensile strength and maximum strength are measured at room temperature as 354 MPa and 522 MPa, respectively. The elongation at break was 23 %. There are no specific applications on the surface of the specimens. The chemical composition of the AA2024-T6 is presented in the **Table 1**.

Table 1: Chemical composition of the AA2024-T6

Element (*w*/%)								
Cu	Mg	Si	Fe	Cr	Mn	Zn	Ti	Al
3.7	1.22	0.5	0.51	0.15	0.32	0.03	0.05	Balance

The specimens were welded with rotary-friction-welding machine. **Table 2** shows the welding parameters used in RFW tests for all experiments, the spindle speed and friction pressure were 1200 min^{-1}, 60 MPa, respectively. The total friction time was adjusted to 8 s, whereas the duration of the forging time was 4 s.

Table 2: Welding parameters employed in RFW experiments

Experiment No.	Forging pressure (MPa)	Friction pressure (MPa)	Forging time (s)	Friction time (s)
1	80	60	4	8
2	100			
3	120			

The specimens were cut from a plane that is parallel to the axis of rotation for metallographic explorations. Conventional metallographic procedures were applied to the joined specimens. The microstructure specimens were etched with Keller solution with an application time of 8 s. A Nikon Eclipse L150A light optical microscope was employed for micro and macrostructural investigations. Also, FEI Quanta 200 FEG scanning electron microscope (SEM) with energy dispersive spectroscopy (EDS) device was employed for metallurgical exploration. A Wilson hardness tester was used for microhardness measurements. Hardness measurements were taken with 0.25-mm intervals with a 10-gF load.

3 RESULTS AND DISCUSSION

The effect of the friction pressure on tensile-elongation behaviour of the rotary-friction-welded AA2024-T6 aluminium joints is shown in **Figure 1**. According to the figure, the tensile strength of the base metal exhibited the best tensile performance among all tensile tests with 472.26 MPa maximum tensile bearing capacity. None of the rotary-friction-welded specimens has achieved the tensile strength of the base metal. Changing the forging pressure during welding has an effect on the tensile strength. The tensile strengths increased as the forging pressure is decreased. The maximum tensile strength is obtained at a forging pressure of 80 MPa. The tensile strengths for forging pressures of (120, 100 and 80) MPa were obtained as 345.37, 359.10, and 366.22, respectively.

The elongations represent the degree of ductility for the material being tested. The elongation has similar characteristics compared to tensile behaviour of the joints. **Figure 2** shows the effect of forging pressures on the elongation at break and failure energies. The elongations were decreased as the forging pressure increases. On the other hand, the base metal has an elongation of 19.21 % that is similar to the elongation at a forging pressure of 80 MPa, achieving 19.28 % elongation. The lowest elongation was obtained in forging pressure of 120 MPa as 15.37 %. There was an approximately 20 % loss in elongation compared to the application pressure of 80 MPa. Namely, there is an important ductility loss in the experiment that has forging pressure of 120 MPa.

The failure energy is another important aspect for evaluating toughness and the energy-absorption capacity

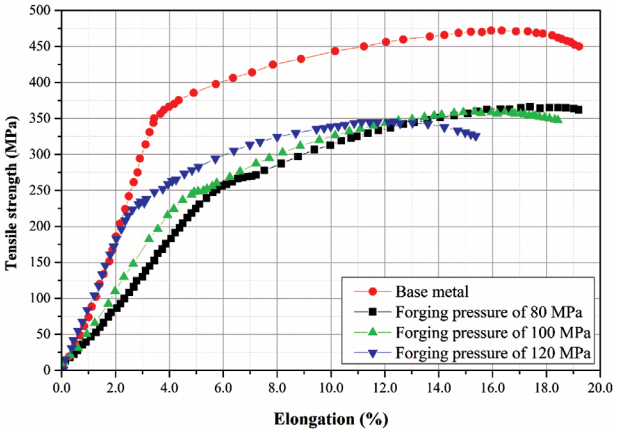

Figure 1: Effect of different forging pressures on tensile strengths

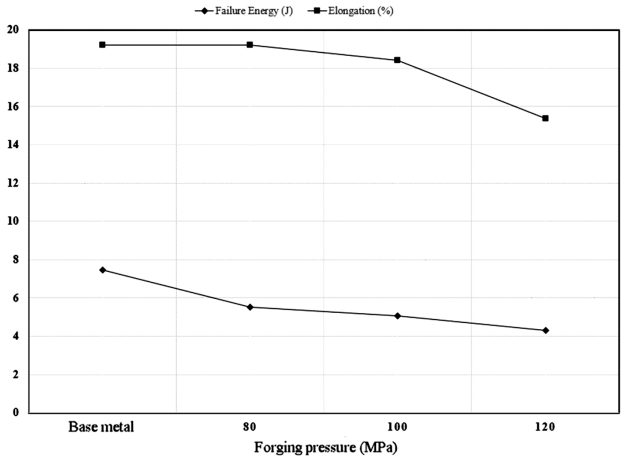

Figure 2: Effect of forging pressure on elongation at break and failure energy

of the joint. Therefore, measuring the failure energy is of great importance. The failure energy was measured with an integration of the area under the tensile-elongation curve. According to the failure-energy results, the maximum failure energy was obtained in the base metal. The failure energy has an inverse relation to the forging pressure. Since the elongation and tensile strength were decreased with an increase in the forging pressure, the failure energies were decreased as the forging pressure increases.

A rotary welded and trimmed microstructure specimen with 80 MPa forging pressure is presented in **Figure 3a** and **3b**. On the other hand, light optical microscope microstructure images from the cross-section of this specimen are presented in **Figures 3c** to **3e**. The microstructure of the rotary-friction-welded AA2024 can be divided into four section for both jointing side; i) base metal (BM), ii) heat-affected zone (HAZ), iii) thermo-mechanically affected zone (TMAZ) and iv) dynamically recrystallized zone (DRZ).

Given the grain size and distribution, BM has a coarse grain size in the microstructure between 10 μm and 240 μm. These grains are not equiaxed and elongated through the rotation axis. Due to the tempering effect, the grains in the HAZ are coarsened as well. With a combination of forging and friction force that is parallel to the rotation axis, the grains are enforced to extend outside. Namely, the elongation axis was deflected 90° due to these effects. The friction heat and dynamic stirring of both friction surfaces causes both recrystallization and mechanical deflection of the grains simultaneously. Therefore, elongated grains perpendicular to the rotation axis and finer grains compared to HAZ are obtained. As for DRZ, this region represents the fusion and solidified zone. Since each side of the specimen is cold, the DRZ underwent quick solidification. Thereby, a finer grain size in the weld joint is obtained.

Line hardness measurement from the cross-section of the rotary-friction-welded joint is illustrated in **Figure 4**. The BM has 117 ± 5 HV hardness. In the HAZ, the hardness increases up to 130 HV due to the tempering effect. Then, the hardness reaches the maximum point in the TMAZ due to the combined effect of strain hardening and tempering. However, as we move into the DRZ, the hardness decreases. Partial recrystallization affects the

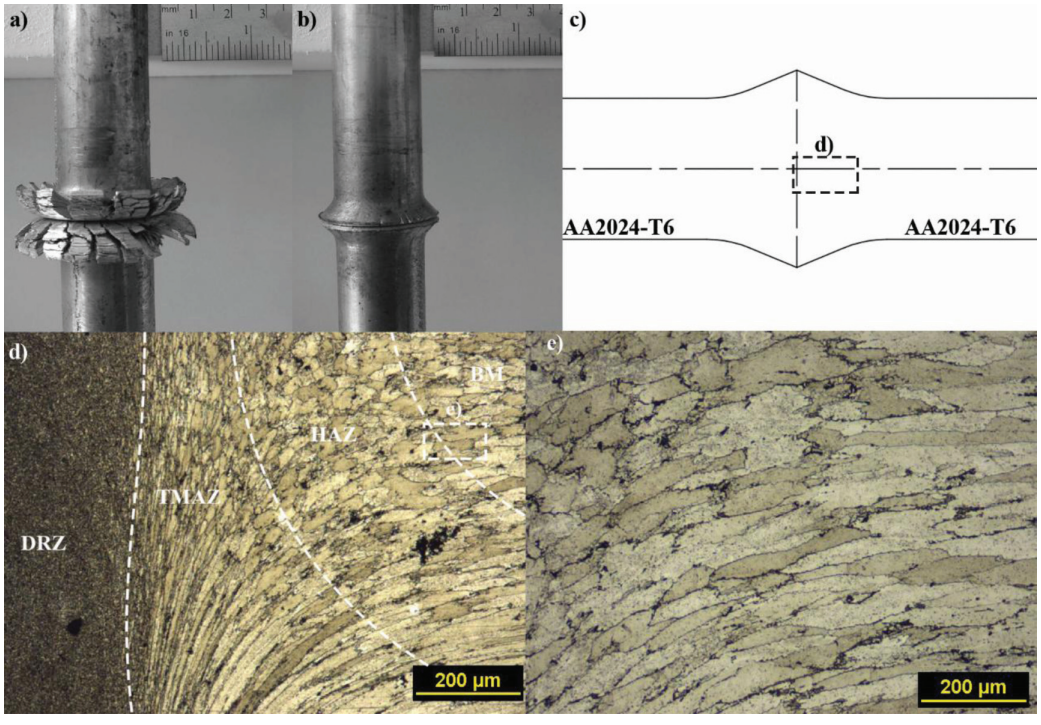

Figure 3: Macro image of a) untrimmed and b) trimmed rotary-friction specimen, c) schematic of the LOM image, microstructure image from d) cross-section and e) HAZ and BM interface

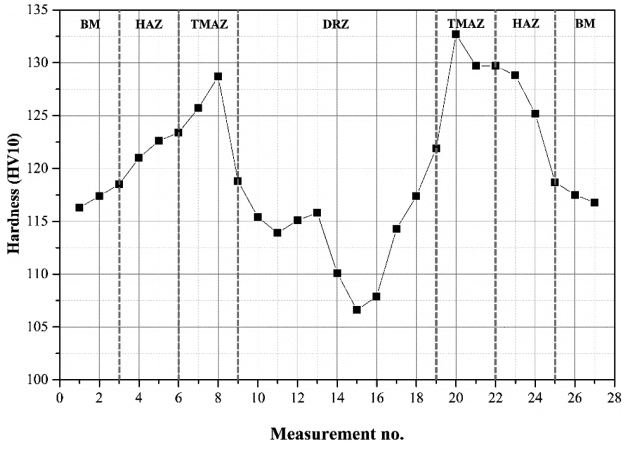

Figure 4: Line hardness measurement from cross-section of the rotary-friction-welded AA2024

strain hardening. As the recrystallization effect increases due to friction heating, the hardness decreases at the same time. This recrystallization ratio reaches a maximum in the DRZ. For this reason, the finer grains were obtained in the DRZ. Although the DRZ has finer grains, the hardness of this region is the lowest. The recrystallized grains had the lowest hardness since these grains are free of strain hardening and tempering effects.

Energy dispersive x-ray spectroscopy (EDS) is a useful technique to characterize the phases in the microstructure. **Figure 5** and **Table 3** show line and point EDS results from the TMAZ. The line EDS measurements were taken from intergranular formations. As seen from the figure, there are some Mg, Cu and Si responses. While the first EDS measurement point exhibited a Si response, 0.04 % of the Si from the second EDS measurement was obtained. The content of the first EDS point

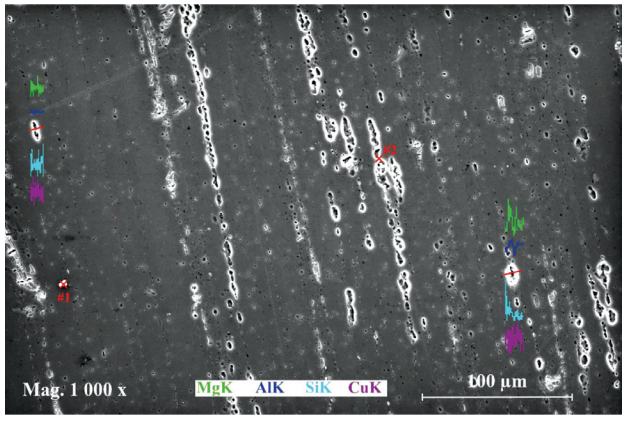

Figure 5: Line EDS and point EDs measurements from TMAZ

Table 3: Point EDS measurement results

Measurement No.	Elements (Conc.-%)			
	Mg	Cu	Si	Al
1	1.68	2.86	0.44	95.02
2	1.87	3.86	0.04	94.22

can be attributed to the presence of Al_2Cu + Al_3Mg_2 + Mg_2Si or Al(CuMgSi) phases. On the other hand, the second EDS result reflects a clear indication of Al_2CuMg (S phase) phase. The S-phase existed the intergranular regions in TMAZ and HAZ. As well as the coarse S phase, the solid-solution clusters that converted into the GPB zones increase the hardness of the HAZ. Due to severe plastic flow and heating, the S phases and GBP zones are coarsened in the TMAZ. The natural aging is the main driving force for the coarsening effect. However, the hardness near the DRZ and in the DRZ decreased since the S-phases and GBP zones are dissolved in the microstructure due to the recrystallization effect. Similar results were also obtained by various researchers. It was reported that the S phases are generally at intergranular locations in the TMAZ.[19] Due to the recrystallization effect stemmed from friction heating, the S phase is dissolved in the grains.

Geng noted that the Al_2CuMg (S) and Al_2Cu (θ) phases are present in the HAZ and TMAZ.[20] These phases are dissolved in the Al matrix of the DMZ due to the heating effect.

4 CONCLUSIONS

In this work, AA2024 aluminium rods were successfully welded with the rotary-friction-welding technique. According to the results, following conclusions can be drawn:

- Friction increased the severity of the heat input in the HAZ and TMAZ, causing wide, brittle regions. These wide HAZ and TMAZ resulted in less tensile strength. Therefore, the forging pressure has an adverse effect on the tensile strength of the RFW specimens.
- Increasing the friction pressure elevated the hardness, especially in the TMAZ region. Brittleness in the DRZ, HAZ and TMAZ caused a local loss of ductility. For this reason, the elongation at break and the failure energy tend to decrease at high friction pressures.
- The Al(CuMgSi) and Al_2CuMg phases are present in the microstructure. Al_2CuMg plays an important role in the strengthening mechanism. These phases precipitated at intergranular locations.
- The amount of Al_2CuMg and other natural aging phases tend to increase near to the DRZ due to the heating effect. Also, the maximum hardness is generally obtained in the TMAZ. However, the hardness is suddenly decreased due to the recrystallization effect induced by welding heat. During recrystallization, the secondary phases are dissolved in the solid solution.
- Since the newly recrystallized grains have a minimum amount of precipitation phases, the lowest hardness is obtained at the DRZ. The main reason for fail-

ure from the DRZ in tensile specimens can be attributed to this softening effect.

5 REFERENCES

[1] I. Morozova, A. Królicka, A. Obrosov, Y. Yang, N. Doynov, S. Weiß, V. Michailov, Precipitation Phenomena in Impulse Friction Stir Welded 2024 Aluminium Alloy, Mater. Sci. Eng. A, 852 (**2022**), 1–11, doi:10.1016/j.msea.2022.143617

[2] S. J. Kalita, Microstructure and Corrosion Properties of Diode Laser Melted Friction Stir Weld of Aluminum Alloy 2024 T351, Appl. Surf. Sci. 257 (**2011**), 3985–3997, doi:10.1016/j.apsusc.2010.11.163

[3] C. S. Wu, W. Bin Zhang, L. Shi, M. A. Chen, Visualization and Simulation of Plastic Material Flow in Friction Stir Welding of 2024 Aluminium Alloy Plates, Trans. Nonferrous Met. Soc. China (English Ed.) 22 (**2012**), 1445–1451, doi:10.1016/S1003-6326(11)61339-3

[4] D. G. Moghadam, K. Farhangdoost, Influence of Welding Parameters on Fracture Toughness and Fatigue Crack Growth Rate in Friction Stir Welded Nugget of 2024-T351 Aluminum Alloy Joints Trans. Nonferrous Met. Soc. China (English Ed.), 26 (**2016**), 2567–2585, doi:10.1016/S1003-6326(16)64383-2

[5] P. L. Niu, W. Y. Li, N. Li, Y. X. Xu, D. L. Chen, Exfoliation Corrosion of Friction Stir Welded Dissimilar 2024-to-7075 Aluminum Alloys, Mater. Charact., 147 (**2019**), 93–100, doi:10.1016/j.matchar.2018.11.002

[6] H. R. Lashgari, S. Li, C. Kong, M. Asnavandi, S. Zangeneh, Rotary Friction Welding of Additively Manufactured 17-4PH Stainless Steel, J. Manuf. Process., 64 (**2021**), 1517–1528, doi:10.1016/j.jmapro.2021.03.008

[7] R. Selvaraj, K. Shanmugam, P. Selvaraj, B. Prasanna Nagasai, V. Balasubramanian, Optimization of Process Parameters of Rotary Friction Welding of Low Alloy Steel Tubes Using Response Surface Methodology, Forces Mech., 10 (**2023**), 1–20, doi:10.1016/j.finmec.2023.100175

[8] F. Jin, J. Li, Y. Du, X. Nan, J. Shi, J. Xiong, and F. Zhang, Numerical Simulation Based upon Friction Coefficient Model on Thermo-Mechanical Coupling in Rotary Friction Welding Corresponding with Corona-Bond Evolution, J. Manuf. Process., 45 (**2019**), 595–602, doi:10.1016/j.jmapro.2019.08.001

[9] T. Dhamothara kannan, P. Sivaraj, V. Balasubramanian, S. Malarvizhi, T. Sonar, M. Ivanov, S. Sathiya, Joining Different Grades of Low Carbon Steel to Develop Unsymmetrical Rod to Plate Joints Using Rotary Friction Welding for Automotive Applications, Forces Mech., 10 (**2023**), 1–18, doi:10.1016/j.finmec.2022.100153

[10] K. Zhang, X. Qian, J. Chen, J. Chen, H. Lu, Non-Monotonic Evolution of Microstructure and Fatigue Properties of Round Bar–Plate Rotary Friction Welding Joints in 304 Austenitic Stainless Steel, Mater. Des., 224 (**2022**), 1–16, doi:10.1016/j.matdes.2022.111400

[11] M. Stütz, R. Buzolin, F. Pixner, C. Poletti, and N. Enzinger, Microstructure Development of Molybdenum during Rotary Friction Welding, Mater. Charact., 151 (**2019**), 506–518, doi:10.1016/j.matchar.2019.03.024

[12] J. S. Chatha, A. Handa, T. S. Bedi, Strength Analysis of Rotary Friction Welded Joints of Dissimilar Steel Grades, Mater. Today Proc., 38 (**2020**), 242–247, doi:10.1016/j.matpr.2020.07.090

[13] A. Anandaraj, S. Rajakumar, V. Balasubramanian, S. Kavitha, Influence of Process Parameters on Hot Tensile Behavior of Rotary Friction Welded In 718/AISI 410 Dissimilar Joints, CIRP J. Manuf. Sci. Technol., 35 (**2021**), 830–838, doi:10.1016/j.cirpj.2021.09.010

[14] T. Tang, Q. Shi, B. Lei, J. Zhou, Y. Gao, Y. Li, G. Zhang, G. Chen, Transition of Interfacial Friction Regime and Its Influence on Thermal Responses in Rotary Friction Welding of SUS304 Stainless Steel: A Fully Coupled Transient Thermomechanical Analysis, J. Manuf. Process., 82 (**2022**), 403–414, doi:10.1016/j.jmapro.2022.08.016

[15] N.K. Mishra, A. Shrivastava, Improvement in Strength and Ductility of Rotary Friction Welded Inconel 600 and Stainless Steel 316L with Cu Interlayer, CIRP J. Manuf. Sci. Technol., 41 (**2023**), 19–29, doi:10.1016/j.cirpj.2022.12.006

[16] K.G. Prashanth, R. Damodaram, S. Scudino, Z. Wang, K. Prasad Rao, J. Eckert, Friction Welding of Al-12Si Parts Produced by Selective Laser Melting, Mater. Des., 57 (**2014**), 632–637, doi:10.1016/j.matdes.2014.01.026

[17] H.K. Rafi, G.D.J. Ram, G. Phanikumar, K.P. Rao, Microstructure and Tensile Properties of Friction Welded Aluminum Alloy AA7075-T6, Mater. Des., 31 (**2010**), 2375–2380, doi:10.1016/j.matdes.2009.11.065

[18] H. Mogami, T. Matsuda, T. Sano, R. Yoshida, H. Hori, A. Hirose, High-Frequency Linear Friction Welding of Aluminum Alloys, Mater. Des., 139 (**2018**), 457–466, doi:10.1016/j.matdes.2017.11.043

[19] P. Li, Y. Jiang, S. Wang, C. Li, H. Sun, B. Wu, H. Dong, J. Zhou, Effect of Post-Weld Heat Treatment on Inhomogeneity of Mechanical Properties and Corrosion Behavior of Rotary Friction Welded 2024 Aluminum Alloy Joint, J. Manuf. Process., 75 (**2022**), 1012–1022, doi:10.1016/j.jmapro.2022.01.059

[20] P. hao GENG, G. liang QIN, J. ZHOU, C. an LI, Parametric Optimization and Microstructural Characterization of Friction Welded Aeronautic Aluminum Alloy 2024, Transactions of Nonferrous Metals Society of China (English Edition), Trans. Nonferrous Met. Soc. China (English Ed.), 29 (**2019**), 2483–2495, doi:10.1016/S1003-6326(19)65156-3